

This paper is a postprint of a paper submitted to and accepted for publication in:

IET Microwaves, Antennas and Propagation, and is subject to Institution of Engineering and Technology Copyright. The copy of record is available at the IET Digital Library

IET Microwaves, Antennas & Propagation

Large Electromagnetic Activity Metamaterial Composed of Five-Segment Cranks

MAP-2018-5900 | Research Article

Submitted by: Angel J Garcia-Collado, Gregorio J Molina-cuberos, Jose Margineda, Ismael Barba

Keywords: METAMATERIALS, CHIRAL MEDIA, POLARIZATION

Large Electromagnetic Activity Metamaterial Composed of Five-Segment Cranks

ISSN 1751-8644
doi: 0000000000
www.ietdl.org

Angel J. García-Collado¹, Gregorio J. Molina-Cuberos², José Margineda², Ismael Barba³

¹ Dpto. Ciencias Politécnicas. Grupo de Teledetección, Geomática y Sistemas de Información Geográfica Aplicados, Universidad Católica de Murcia, E-30107 Murcia, Spain

² Dpto. de Electromagnetismo y Electrónica, Universidad de Murcia, E-30100 Murcia, Spain

³ Dpto. de Electricidad y Electrónica, Universidad de Valladolid, E-47071 Valladolid, Spain

* E-mail: ajgarcia@ucam.edu

Abstract: A new chiral material composed of a two-dimensional lattice of five-segment cranks, with the same handedness is experimentally and numerically studied. The sample, formed by a single layer of such structures, exhibits huge electromagnetic activity and a negative refraction index for linearly polarized waves. Both the chirality parameter and the bandwidth with the negative refraction index are larger than those observed in chiral media composed of three-segment cranks. The material also shows pronounced electromagnetic activity (larger than 500° per wavelength). This observed behaviour is attributed to the fact that the five-segment configuration enhances the electromagnetic coupling compared with the three-segment configuration.

1 Introduction

The ability of some media to rotate the polarization plane of a linearly polarized wave (LPW), known as optical activity, was discovered in 1815 by Jean-Baptiste Biot. Some years later, Louis Pasteur [1] observed the same effect in tartaric acid salts and found that sodium tartrate and ammonium, both optically inactive, were present as a mixture of two different kinds of crystal, each a mirror image of the other. After separating the mixture into two parts, each was seen to contain molecules with the same spatial symmetry, so that each part was optically active. Furthermore, the specific rotations of both solutions had the same magnitude and opposite sign; i.e., if a solution rotated the linearly polarized light to the right, the other one rotated an equal number of degrees to the left. In all other properties, both substances were identical. As a consequence, a racemic solution with an equal number of crystals of both types does not produce any rotation. The change in the direction of polarization is known as optical rotary dispersion. Another possible effect in such a medium is circular dichroism, when a linear polarized wave becomes elliptical.

The wavelength of the optical activity phenomenon is determined by the size of the molecule. The most common cases of chiral activity in nature, as the one described by Pasteur, appear in the visible region of the spectrum. To date, no natural material capable of producing the same effect at microwave frequencies has been found, although several artificial structures have been designed and built with such an aim. The first one was developed at the end of the nineteenth century [2]. When the activity phenomenon occurs at microwave frequency, it is said that the material presents electromagnetic activity.

The size of the metallic helices determines the frequency band where the chiral effect appears [3]. In the 1990s the resonant frequency was increased by decreasing the size of the helices [4]. By using chiral cranks made from conducting wires folded in three segments, García-Collado et al. [5] demonstrated that a random distribution of non-helical structures was able to produce electromagnetic activity.

To date, several research groups have designed a variety of structures with electromagnetic activity ranging from a few GHz to THz. The present manufacturing method, which strongly enhances the electromagnetic response, makes use of a printed circuit board to design the chiral structures, which are repeated in a two dimensional

network [6]. This technique allows a tighter control and greater precision than is possible with the random distribution and making the media more reproducible. Due to the bidimensional arrangement and the symmetry properties of the resonator, the materials are anisotropic for non perpendicular incident beams. Several structures have been designed to produce strong electroagnetic activity and circular dichroism, such as twisted rosettes [7], split ring resonators [8], cross-wires [9], twisted metallic foil [10], L-shaped resonators [11], U-shaped resonators [12], etc.

Furthermore, it has been observed that in media with high electromagnetic activity, at certain frequencies and a narrow bandwidth, their behaviour is similar to that of a homogeneous material of negative index of refraction, without the values of permittivity and permeability being simultaneously negative. Negative refraction materials have acquired increasing importance because of their interesting electromagnetic properties and potential applications, such for cloaking [13], subwavelength imaging [14], optical storage [15], and in polarization devices [16].

Here, we present an evolution of the three-segment crank resonator, whose basic cell consists of two or four packed three-dimensional metallic cranks, all with the same symmetry, forming a parallelepiped [17]. The new chiral material is composed of a two-dimensional lattice of five-segment cranks. This five-segment configuration presents stronger electromagnetic coupling, which produces higher chirality effects as well as a wider frequency band with a negative refractive index compared with three-segment cranks.

2 Methods

2.1 Sample and experimental system

Figure 1 shows some schematic drawings of the structure and the unit cell. As can be seen, two of the segments are on the front face of the dielectric substrate, forming an angle of 90° to each other, and two more are on the back face side of the substrate, with the same geometry and rotated 180° with respect to those on the front face. The last metallic conductor is a cylindrical path that crosses the substrate and connects the segments located on both faces of the dielectric slab. Before building the samples, several simulations were performed using a commercially available simulator (CST Microwave Studio®). Such numerical modelization provide information on the dependence of the resonant frequencies on the

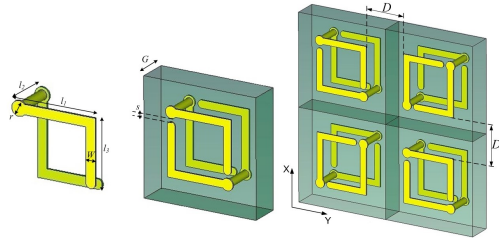


Fig. 1: (a) Five-segment crank, (b) crank resonator composed of two same handedness cranks, and (c) unit cell. The geometric parameters are given by: $\ell_1 = 3.58$ mm, $\ell_2 = 2.40$ mm, $\ell_3 = 2.45$ mm, $W = 0.50$ mm, $s = 0.40$ mm, $L = 2.40$ mm, $D = 3.45$ mm. The total crank length is $l_T = 2\ell_1 + \ell_2 + 2\ell_3 = 14.46$ mm.

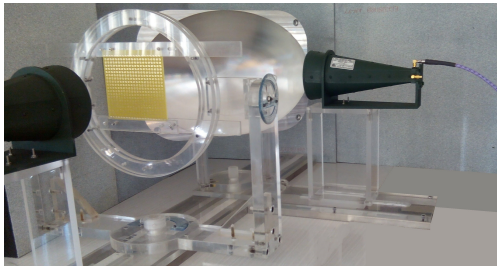


Fig. 2: Measurement setup with the chiral material in the circular sample holder.

geometrical parameters of the structure, and ensured that the resonant frequencies are within the experimental frequency range (from 6 GHz to 18 GHz). We have simulated the normal incidence of a plane wave over a infinite 2D arrangement of unit cells to calculate the T_{xx} , T_{yx} and R coefficients. The caption of Figure 1 shows the geometrical dimensions used in this paper. The tracks are $35 \mu\text{m}$ thick, and the dielectric substrate is a FR-4 standard board, with an electric permittivity of $\epsilon_r = 4.3$, loss tangent of 0.025 and 2.4 mm width at 10 GHz.

The combination of two five-segment cranks, with the same handedness and rotated together 180° about an axis passing through the centre of the structure, perpendicular to the substrate surface, constitutes a resonator. This structure has three binary symmetry axes. In order to achieve a homogeneous bi-isotropic behaviour for normal incident waves, it is necessary to increase the C_2 symmetry to reach C_4 symmetry. The unit cell is composed of four resonators, each rotated by 90° with respect to the neighbouring ones, in such a way that the system remains invariant after 90° rotations around the z -axis. An outline of the unit cell is presented in Fig. 1(c), where the configuration now has four binary symmetry axes in the xy -plane and also an axis of quaternary symmetry in the z -axis direction.

The experimental system is based on a previous one constructed for chiral characterization in X-band [18], and adapted to extend the frequency range from 6 to 18 GHz, Fig. 2. The setup consists of a two-port network analyser connected by coaxial cable to two dual horn antennae. The incident beam is focused by an ellipsoidal concave mirror so that diffraction problems with relatively small samples are avoided [19]. The transmitting antenna is placed at one

of the mirror foci and the sample at the other one. The two ports of the polarized receiving antenna allow the transmission coefficients to be measured in two perpendicular directions.

The entire measurement system is constructed of non-conductive material, and allows mechanical regulation. In order to determine the transmitted and reflected signals, the reference planes must be located at the sample faces, so that normalization relative to the incident signal is necessary. The complete process involves measurement of the reflected and transmitted wave with the sample, the transmitted signal without the device under test, and the reflected signal when the sample is substituted by a metallic plane with the same dimensions and at the same place [18]. The measurements were filtered to remove mismatches and unwanted reflections from the antennae and edge any diffraction effects of the sample, mirrors or elsewhere.

Martín et al. [20] demonstrated that the retrieval of κ does not require the plane to be displaced when circularly polarized waves (CPW) are used and, therefore, two single measurements of the transmission coefficient are necessary.

2.2 Retrieval Algorithm

The goal of electromagnetic characterization is to determine the material parameters, usually the electrical permittivity, ϵ_r , and the magnetic permeability, μ_r . For homogeneous and isotropic media, the constitutive equations can be written as $\vec{D} = \epsilon_0 \epsilon_r \vec{E}$, $\vec{B} = \mu_0 \mu_r \vec{H}$, where ϵ_r and μ_r are two complex frequency-dependent parameters. However, chiral materials present an electromagnetic coupling between the electric and magnetic fields and do not follow to the above equations. In order to describe macroscopically their electromagnetic response, a coupling parameter should be included in the constitutive relations [21]:

$$\vec{D} = \epsilon_0 \epsilon_r \vec{E} - j \sqrt{\epsilon_0 \mu_0} \kappa \vec{H}, \quad (1)$$

$$\vec{B} = \mu_0 \mu_r \vec{H} + j \sqrt{\epsilon_0 \mu_0} \kappa \vec{E}, \quad (2)$$

where κ is a frequency-dependent, dimensionless parameter named chirality. The presence of κ increases the complexity of the chiral media characterization.

Chirality implies a coupling between the electric and magnetic fields and, therefore, they cannot be separated in the usual expression of the wave equation. For linearly polarized incident waves, the problem can be overcome by splitting the wave into two circularly polarized waves, with equal amplitude, one left-handed (LCP) and the other right-handed (RCP). These two circular polarized waves are the eigenmodes in a chiral medium [21]. Each polarization propagates through the medium as in an isotropic and homogeneous material, with a refractive index and wave number that can be expressed by [21]:

$$n_{\pm} = n \pm \kappa = n (1 \pm \kappa_r) = \sqrt{\epsilon_r \mu_r} (1 \pm \kappa_r), \quad (3)$$

$$k_{\pm} = \frac{\omega}{c} \sqrt{\epsilon_r \mu_r} (1 \pm \kappa_r) = k_0 (n \pm \kappa), \quad (4)$$

where $n = \sqrt{\epsilon_r \mu_r}$ is the refractive index, $k_0 = \omega/c$ the free space wave number, and $\kappa_r = \kappa / \sqrt{\epsilon_r \mu_r}$ the relative chirality. + and - represent the clockwise and anticlockwise modes, respectively.

The material refractive index can be calculated from experimental data by [18]:

$$n = \frac{-j}{2k_0 L} \ln \left| \frac{R - \Gamma}{R\Gamma^2 - \Gamma} \right| + \frac{1}{2k_0 L} \arg \left(\frac{R - \Gamma}{R\Gamma^2 - \Gamma} \right) + \frac{\pi}{k_0 L} m, \quad (5)$$

where Γ is a function of the measured (or simulated) transmission (T_{xx} and T_{yx}) and reflection (R) coefficients. Γ is related with the relative impedance $z_r = \sqrt{\mu_r / \epsilon_r}$, by $\Gamma = (1 + z_r) / (1 - z_r)$ [18], L the slab width and m is an integer related to the branch of the logarithm function, which is determined by assuming a known behaviour far from the resonance and that both the real and imaginary parts of n resonate at the same frequency.

The electrical permittivity and magnetic permeability are calculated by:

$$\varepsilon_r = \frac{n}{z_r}, \quad (6)$$

$$\mu_r = n z_r. \quad (7)$$

The chirality parameter can be calculated from the transmission experimental data [18] by:

$$\kappa = \frac{j}{2k_0L} \ln \left| \frac{T_{++}}{T_{--}} \right| + \frac{1}{2k_0L} \arg \left(\frac{T_{++}}{T_{--}} \right) + \frac{2\pi}{k_0L} p, \quad (8)$$

where $T_{++} = T_{xx} - jT_{yx}$ is the transmission coefficient for RCP waves, $T_{--} = T_{xx} + jT_{yx}$ the transmission coefficient for LCP waves, and p is an integer that is determined using continuity conditions and considering that both the real and the imaginary part of κ resonate at the same frequency.

Finally, the rotation angle for a linearly polarized incident wave θ and the ellipticity η of the transmitted wave can be calculated by [9]:

$$\theta = \frac{1}{2} \arg \left(\frac{T_{++}}{T_{--}} \right), \quad (9)$$

$$\eta = \frac{1}{2} \sin^{-1} \left(\frac{|T_{++}|^2 - |T_{--}|^2}{|T_{++}|^2 + |T_{--}|^2} \right), \quad (10)$$

where zero η corresponds to linear polarization, 45° corresponds to RCP and -45° corresponds to LCP. Equations (8, 9, 10) show that by measuring T_{--} and T_{++} , it is possible to determine κ , θ and η [20].

3 Results and Discussion

Figure 3 shows the magnitude of the transmission and reflection coefficients for LPW as well as the transmission coefficients for RCP and LCP. In order to validate the simulation model, the reflection and transmission coefficients obtained by simulations have been plotted in Fig. 3. The good agreement observed between experimental and numerical data supports the results obtained by simulations as described below.

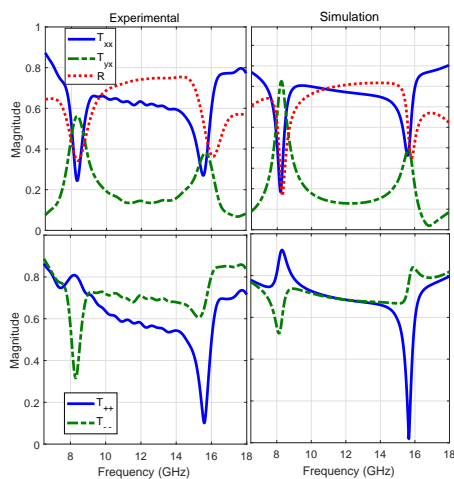


Fig. 3: Experimental (left column) and simulation (right column) results of the reflection and transmission coefficients for linear (top file) and circular (bottom file) polarized waves.

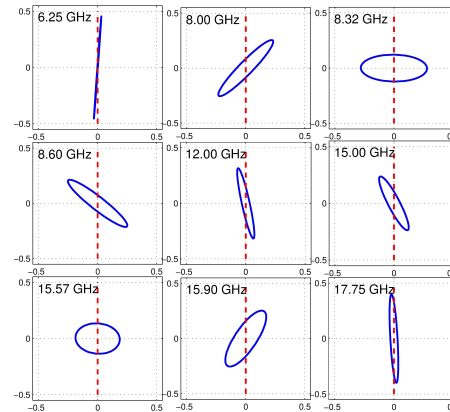


Fig. 4: Polarization ellipse of the signal transmitted at different frequencies (solid blue line) and incident wave (dashed red line).

The first resonance, f_1 , is placed at 8.3 GHz and the second resonance, f_2 , at 15.6 GHz. Using simulations it was found that f_1 is inversely proportional to the crank total length, which is typically observed in random distribution-based chiral media [3], and is almost independent of the separation between units cells.

For the first resonance, and considering the experimental values, the minimum value of $|T_{xx}|$ is 0.24 at 8.33 GHz, and the maximum of $|T_{yx}|$ is 0.56 at the same frequency, which indicates a change in the polarization state of the signal, which is transformed after transmission from linear to elliptical and a rotation in the polarization plane of the transmitted wave. To discern both effects it is necessary to take into account the phase difference between T_{++} and T_{--} , by using (9, 10). The reflection coefficient $|R|$ depends on the frequency following a similar pattern to that observed for $|T_{xx}|$, reaching a minimum value of 0.34.

It can be seen that at f_1 , $|T_{--}|$ reaches a minimum and $|T_{++}| > |T_{--}|$, and so the transmitted signal is anticlockwise. By contrast, at frequencies above about 9 GHz the transmitted signal is clockwise, $|T_{--}| > |T_{++}|$, and the difference in magnitude is larger at the second resonance, where $|T_{++}|$ reaches a minimum.

One way to visualize the changes in the polarization is by plotting the polarization ellipse of the transmitted signal for a given frequency. Fig. 4 shows the results for nine selected frequencies and where the incident signal is also plotted. Far from the first resonance, $f = 6.25$ GHz, the polarization is almost linear, which corresponds to $\eta \approx 0$. As the frequency increases and approaches the first resonance region, the polarization changes from linear to elliptical. For f_1 and f_2 , the transmitted signal has been rotated an angle of $\approx 90^\circ$ and is clearly elliptical. Far from the second resonance, at 17.75 GHz, the transmitted wave recovers linear polarization. From this plots it is clear that the chiral material presents both rotary optical dispersion and circular dichroism.

Numerical simulation enables the examination of the field distribution inside the unit cell. Fig. 5 shows electric and magnetic field energy in both faces of a sample at the first resonant frequency. We can see how both fields are concentrated in the region inside the two-crank resonators, labelled 2 and 4. Indeed, simulations performed removing resonators 1 and 3 lead to minor changes in the scattering parameters, assuming the initial polarization of the incident wave does not change. This may be caused by the orientation of the different cells: in cells 1 and 3 the vertical segments short-circuit the incident field, while 2 and 4 show a capacitive answer. If the incident wave is horizontally polarized, the fields are concentrated on resonators 1 and 3 instead.

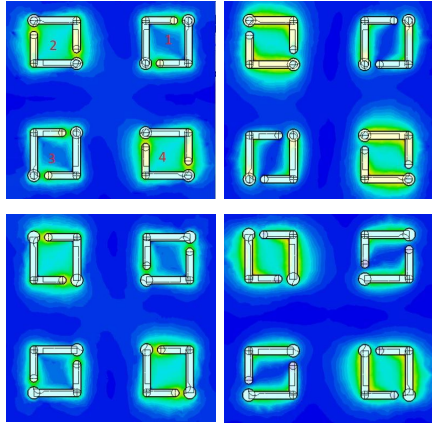


Fig. 5: Top plots: Electric (left) and magnetic (right) energy density at the incidence face. Bottom plots: Electric (left) and magnetic (right) fields at the transmission face. The incident wave is polarized in the vertical direction with a frequency of 8.25 GHz.

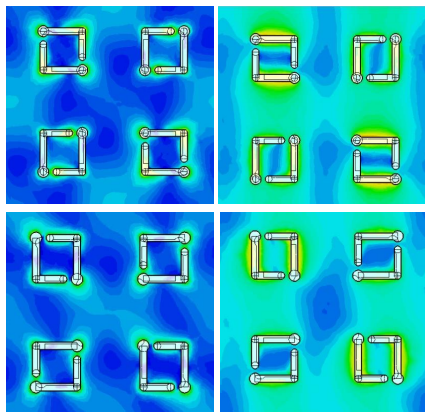


Fig. 6: Top plots: Electric (left) and magnetic (right) energy density at the incidence face. Bottom plots: Electric (left) and magnetic (right) fields at the transmission face. The incident wave is polarized in the vertical direction with a frequency of 15.64 GHz.

Figure 6 shows electric and magnetic field energy in both faces of a sample at the second resonant frequency. In this case, there is a magnetic field in the space between cells. More simulations show that the second resonance strongly depends on the distance between resonators, while the first frequency depends mainly on the crank total length.

Figure 7 shows the retrieved values of the rotation angle, ellipticity, refractive indices, chirality, permittivity and permeability obtained from experimental data. As can be seen, both the rotation angle θ and the ellipticity η peak at the resonant frequencies. For $f_1 = 8.33$ GHz and $f_2 = 16.67$ GHz, the transmitted wave has rotated $\theta = \pm 90^\circ$ with respect to the incident one and the polarization has changed to elliptical. There are also discontinuities in

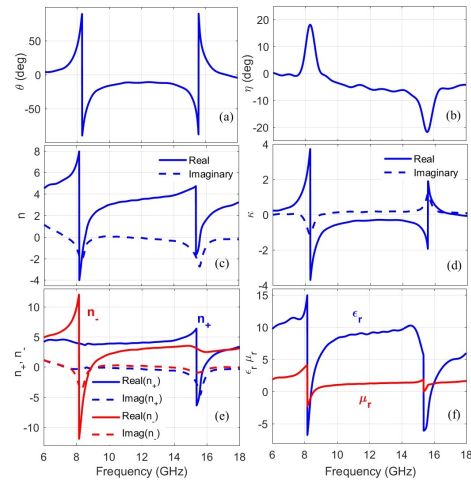


Fig. 7: Retrieved values for the (a) rotation angle, (b) ellipticity, (c) refractive index n , (d) chirality parameter, (e) refractive index for the two circularly polarized waves, n_+ and n_- , (f) relative permittivity and relative permeability, where the real and imaginary parts are plotted as solid and dashed lines, respectively. All the parameters have been calculated from experimental data.

the resonances, where the θ jumps 180° in magnitude. The transmitted signal presents elliptical polarization with extreme values of $\eta_{min} = 18^\circ$ at f_1 and $\eta_{min} = -22^\circ$ at f_2 . From 10 to 14 GHz, the transmitted signal maintains an almost linear polarization, forming an angle of around $\theta = 10^\circ$ with respect to the incident wave. Using simulations and changing the geometrical parameters of the structure, the rotation angle can be increased up to $\theta \approx 45^\circ$, for a bandwidth of around 3 GHz and keeping a low ellipticity, $\eta < 5^\circ$. This means pure electromagnetic activity (electromagnetic activity with η near to zero) of $\approx 450^\circ$ per wavelength (at 10 GHz), which is larger than that obtained by Kenanakis [22] in a comparative study of five different chiral metamaterials.

Figures 7(c) and 7(d) show the real and imaginary parts of the refractive index (n_+ , n_- and n). At f_1 the real part of the refractive index of left circularly polarized waves, $\Re(n_-)$, presents an abrupt change and the imaginary part a peak, $\Im(n_-) \approx 4$, which means strong absorption of the clockwise mode. However, both the real and imaginary parts of n_+ remain constant and, therefore, the transmitted wave is counterclockwise. The opposite effect occurs at f_2 and there is strong absorption on the right circularly polarized wave, while the transmitted wave presents an ellipticity in the clockwise direction.

It can be observed that the material presents negative refraction for some of the refractive indices for frequencies higher than f_1 : $\Re(n) < 0$ for a 350 MHz bandwidth and $\Re(n_-) < 0$ for a 800 MHz bandwidth. The first case is due to both $\epsilon_r < 0$ and $\mu_r < 0$, while the case of n_- is due to $|\kappa| > |n|$ and $\kappa < 0$, and not to the fact both permittivity as well as permeability are negative, as in traditional negative refraction index materials. In contrast to n_- , the value of n_+ remains nearly constant, with an almost zero imaginary part, i.e. very low absorption.

The observed negative refraction bandwidth for one of the circular polarized waves results in a factor of two, which is larger than that obtained using the three-crank resonator [17].

The retrieved values of κ , ϵ_r and μ_r present discontinuities at the resonant frequencies, Fig. 7(d) and 7(e). Chirality follows a frequency-dependent behaviour similar to that found in chiral materials based on three-segment cranks [17]. However the inclusion of two extra segment enhances the electromagnetic coupling and

increases the value of κ to reach a peak of $\kappa = 3.7 - 1.1j$, which is larger than that of three-segment cranks, $\kappa = 2.6 - 0.85j$ [17].

4 Conclusions

The electromagnetic activity of a chiral metamaterial based on crank structures has been improved by including an extra two segments in a previous three-segment crank design. We have studied, both numerically and experimentally, the transmission and reflection of linear and circular propagating waves and calculated the effective parameters and electromagnetic activity. The new five-segment crank produces a stronger coupling between the electric and magnetic fields and therefore, represents a clear improvement over the previous structure. Among the findings were a higher chirality parameter, double negative permittivity and permeability and a factor of two larger bandwidths with negative refractive index for one of the circular polarized waves. The existence of two resonance frequencies within the study band was checked. At both these frequencies the chirality present an abrupt change reaching extreme values, the rotation angle reached 90° and the ellipticity also showed maximum absolute values. The large optical activity of $\approx 500^\circ$ per wavelength (at 10 GHz) makes our design a valuable candidate for the development of GHz manipulation components such as wave-plates and circular polarization filters.

5 Acknowledgements

This work has been supported by the Ministerio de Economía y Competitividad of Spain (Research Projects TEC2014-55463-C3-1-P and TEC2014-55463-C3-3-P) and by the European Commission (ERDF).

6 References

- [1] Pasteur, L.: 'Recherches sur les relations qui peuvent exister entre la forme cristalline, la composition chimique et les sens de la polarisation rotatoire' (Impr. Bachelier, 1848)
- [2] Bose J.C.: 'On the rotation of plane of polarisation of electric waves by a twisted structure', Proc. Roy. Soc., 1898, 63, pp. 146–152
- [3] Tinoco, I., Freeman, M.P.: 'The Optical Activity of Oriented Copper Helices. I. Experimental', J. Physical Chemistry, 1957, 61, pp. 1196–1203
- [4] Ro, R., Varadan, V.V., Varadan, V.K.: 'Electromagnetic activity and absorption in microwave chiral composites', IEE Proceedings H (Microwaves, Antennas and Propagation), 1992, 139(5), pp. 441–448
- [5] García-Collado, A.J., Molina-Cuberos, G.J., Margineda, J., et al.: 'Isotropic and homogeneous behavior of chiral media based on periodical inclusions of cranks', Microwaves and Wireless Components Letters, 2010, 20(3), pp. 176–177
- [6] Barba, I., Cabeceira, A.C.L., García-Collado, A.J., et al.: 'Quasi-planar Chiral Materials for Microwave Frequencies', in Electromagnetic Waves Propagation in Complex Matter, (InTech, 2011, Rijeka, Croatia, pp. 97–116)
- [7] Rogacheva, A.V., Fedotov, V.A., Schwanecke, A.S., et al.: 'Giant gyrotropy due to electromagnetic-field coupling in a bilayered chiral structure', Phys. Rev. Lett., 2006, 97, pp. 177401
- [8] Marqués, R., Mesa, F., Martel, J., et al.: 'Comparative analysis of Edg- and Broadside- Coupled Split Ring Resonators for Metamaterial Design. Theory and Experiments', IEEE Trans. on Antennas and Propagation, 2003, 51(10), pp. 2572–2581
- [9] Zhou, J., Dong, J., Wang, B., Koschny, T., et al.: 'Negative refractive index due to chirality', Phys. Rev. B, 2009, 79, pp. 121104
- [10] Wu, Z., Zeng, B.Q., Zhong, S.: 'A double-layer chiral metamaterial with negative index', J. of Electromagnetic Waves and Applications, 2010, 24(7), pp. 983–992
- [11] Li, J., Yang, F.-Q., Dong, J.-F.: 'Design and simulation of L-Shaped chiral negative refractive index structure', Progress In Electromagnetics Research, 2011, 116, pp. 395–408
- [12] Xiong, X., Sun, W., Bao, Y., et al.: 'Construction of a chiral metamaterial with a U-shaped resonator assembly', Phys. Rev. B, 2010, 81, pp. 075119
- [13] Cheng, X., Chen, H., Zhang, X.-M., et al.: 'Cloaking a Perfectly Conducting Sphere with Rotationally Uniaxial Nihilicity Media in Monostatic Radar System', Progress In Electromagnetics Research, 2010, 100, pp. 285–298
- [14] Jin, Y., He, S.: 'Focusing by a slab of chiral medium', Optics Express, 2005, 13(13), pp. 4974–4979
- [15] Liu, H., He, S.: 'Near-field optical storage system using a solid immersion lens with a left-handed material slab', Optics Express, 2004, 12(20), pp. 4835–4840
- [16] Navarro-Cia, M., Beruete, M., Falcone, F.J., et al.: 'Polarization-tunable negative or positive refraction in self-complementariness-based extraordinary transmission prism', Progress In Electromagnetics Research, 2010, 103, pp. 101–114
- [17] García-Collado, A.J., Molina-Cuberos, G.J., Núñez, M.J., et al.: 'Negative Refraction of Chiral Metamaterial Based on Four Crank Resonators', Journal of Electromagnetic Waves and Applications, 2012, 26(7), pp. 986–995
- [18] Margineda, J., Molina-Cuberos, G.J., Núñez, M.J., et al.: 'Electromagnetic Characterization of Chiral Media', in *Electromagnetic Waves Propagation in Complex Media*, (InTech, 2012, Rijeka, Croatia, pp. 3–24)
- [19] Rojo, M., Munoz, J., Molina-Cuberos, G.J., et al.: 'Design of an ellipsoidal mirror for freewave characterization of materials at microwave frequencies', Measurement Science and Technology, 2016, 27(3), pp. 035001
- [20] Martín, E., Munoz, J., García-Collado, A.J., et al.: 'Chiral retrieval method based on right circularly polarized and left circularly polarized waves', Meas. Sci. Technol., 2014, 25(11), pp. 11500
- [21] Lindell, I.V., Sihvola, A.H., Tretyakov, S.A., et al.: 'Electromagnetic waves in chiral and bi-isotropic media' (Artech House, 1994, Boston, USA)
- [22] Kenanakis, G., Zhao, R., Stavrinidis, A., et al.: 'Flexible chiral metamaterials in the terahertz regime: a comparative study of various designs', Opt. Mater. Express, 2012, 2(12), pp. 1702–1712